DIHEDRAL TILINGS OF THE SPHERE BY REGULAR POLYGONS AND QUADRILATERALS I: SQUARES AND RHOMBI

Hoi Ping Luk*[1]

[1]*Katedra matematiky, Západočeská univerzita v Plzni, Plzeň, Czech Republic*
hoi@connect.ust.hk

Submitted: Nov 14, 2023; Accepted: Apr 28, 2025; Published: Sep 15, 2025

Abstract. We classify the edge-to-edge dihedral tilings of the sphere by squares and rhombi and develop a method that can be applied to future problems.

Keywords. Classification, spherical tilings, dihedral tilings, quadrangulations, division of spaces

Mathematics Subject Classifications. 05B45, 52C20, 51M10, 51M20, 52B10

1. Introduction

Tilings hold lasting fascinations. Beyond aesthetic appeal, they play a key role in solving real-world problems, including many in chemistry, life sciences, and engineering. However, our knowledge of tilings is limited as the studies often face challenges. The recent breakthroughs in long-standing open problems are testaments to the predicament; the discovery of aperiodic monotile of the plane [SMKGS24] and a complete classification of spherical tilings [AWY22, AY23, CL21, CLY22, CLY23, GSY13, LC24, UA02, WY22a, WY22b] came as voluminous efforts.

A *tiling* of a surface is a covering of the surface by tiles without holes and overlaps. The *tiles* are simple polygons, i.e., shapes with geodesic edges such that the boundaries formed by their edges are simple closed curves. If all the tiles are congruent, the tiling is called *monohedral*; if some tiles are congruent to a polygon while the others are congruent to a different polygon, the tiling is called *dihedral*. The congruence classes of the tiles are called *the prototiles* of the tiling. In other words, a monohedral tiling has exactly one prototile, whereas a dihedral tiling has

*The research was supported in part by the funding of Academic Career in Pilsen 2024 under Plzeňský kraj a Západočeská univerzita v Plzni.

exactly two. In general, a tiling with more than one prototile is called *multihedral*. *Vertices* are where the edges meet. A tiling is called *edge-to-edge* if it has no vertex in the interior of an edge, otherwise it is called *non-edge-to-edge*. The *degree* of a vertex counts the number of incident edges. We assume each vertex to have degree $\geqslant 3$ to avoid trivial examples from artificial additions of degree 2 vertices in edges. We do not assume convexity in the prototiles. We also do not assume symmetry in the tilings. In the aforementioned classification, not imposing these conditions often leads to surprising results.

Edge-to-edge tilings of the sphere by regular polygons can be obtained via projection from the Platonic solids (monohedral) [Yoo12], the Archimedean solids (multihedral) [AHS18, Yoo12], the circumscribable Johnson–Zalgaller solids (multihedral) [AHS18, Joh66, Zal67] as well as the infinite series of prisms and antiprisms [AHS18]. A classification of the non-edge-to-edge ones is given in [AEHJ24]. Beyond regular prototiles, the studies become complicated.

From now on, by *tilings* we exclusively mean edge-to-edge tilings of the sphere unless otherwise specified.

The prototile of a monohedral tiling is either a triangle, a quadrilateral or a pentagon, as a result of Euler's polyhedral formula. Tilings with a triangle prototile were first studied by D. Sommerville in 1923 [Som24]. A classification of these tilings was completed in a seminal paper [UA02] by Y. Ueno and Y. Agaoka almost eight decades later. Encouraged by the success, classifications of tilings with a quadrilateral prototile or those with a pentagon prototile were eventually completed through the series [AWY22, AY23, CL21, CLY22, CLY23, GSY13, LC24, WY22a, WY22b]. A posteriori, the challenges in the latter two prototiles are reflected in the volume and the machinery required.

This paper is the first of a series to embark on new classifications and naturally we consider edge-to-edge dihedral tilings of the sphere. The majority of existing results in dihedral tilings specialised in folding type, meaning that such tilings must have a triangle prototile [AS09, BR12, BS05, BRS09]. They are not what we intend to study. Tilings with combinations of non-triangular prototiles are largely understudied. Empirically, they often emerge as an intermediate step in the studies of those with a triangular prototile [CLY22, UA02]. As a natural progression from the regularity in prototiles, the series focuses on the two-prototile combinations consisting of a regular polygon (n-gon) and a rhombus. The prototiles are equilateral, and hence more manageable. Despite that, to the author's knowledge, a systematic study in this direction is lacking.

This paper focuses on $n = 4$ (the square). The sequel [CL24] handles the regular n-gons for $n \geqslant 5$ and a working manuscript addresses $n = 3$.

The prospect of extending the machinery in [CLY22] gives another motivation for this paper. Combinatorially, a dihedral tiling by squares and rhombi has a 1-skeleton with facial cycles of length 4. The same combinatorial tools from the monohedral counterpart ($n = 4$) naturally apply. Geometrically, the square and the rhombus are related via a deformation that preserves the edge length, and hence the same geometric tools on the prototiles also apply.

This paper is also motivated by a parity phenomenon; an edge-to-edge tiling of the sphere by congruent polygons has an even number of tiles. The reason is simple at a combinatorial level when the prototile is a triangle or a pentagon; when the prototile is a quadrilateral, further geometric arguments are required [CLY22, Luk24, Luk25]. It leads to a question on the existence of tilings by the smallest odd number of quadrilaterals with the fewest prototiles. Our choice of

prototiles here gives a negative answer that shortens the search in [Luk25].

From now on, by *dihedral tilings* or simply *the tilings* we mean specifically the edge-to-edge dihedral tilings of the sphere by squares and rhombi.

The contents are organised as follows. In Section 2, we explain the main result. In Section 3, we introduce the terminology and establish the tools. In Section 4, we classify the tilings: the isolated ones in Propositions 4.2, 4.3, 4.4, 4.5, and the infinite family in Proposition 4.6. In Section 5, we discuss the strategy, some interesting phenomena, and some "near misses".

2. Main result

Both prototiles in this paper, referred to as *the square* in Figure 2.1a and *the rhombus* in Figure 2.1b, have edge combination x^4. Their angle configurations are α^4 and $\beta\gamma\beta\gamma$ respectively. These notations are implicitly assumed throughout the paper and the shaded tiles are always the squares.

(a) The square. (b) The rhombus.

Figure 2.1: The two prototiles.

To explain the main result, we borrow concepts from the monohedral tilings. The monohedral tilings can be categorised as the earth map tilings, the Platonic tilings, and the sporadic tilings, together with the associated subdivisions and modifications [LCY24]. An *earth map tiling* is composed of identical copies of a "building block", which is a cluster of tiles. Such a building block is called a *time zone* and its tiles can be viewed as the "countries" within the same time zone. For example, in Figure 2.2 the two tiles (two rhombi, $\uparrow$'s converge to a vertex, same for $\downarrow$'s) with dot pattern form a time zone of the tiling, which consists of three time zones. All the time zones share two common vertices, which in general can be of an arbitrarily high degree depending on the number of time zones. The two vertices are regarded as the "north pole" and the "south pole". In the example, $\uparrow$'s point to the former and $\downarrow$'s point to the latter. The family of tilings given by the time zones is denoted by $E^R_\square 1$ (R for rhombus). For more details, we refer the reader to [CLY22, Proposition 23]. Such tilings resemble the earth map and hence the name. In terms of combinatorial curvature on graphs (see definition in [Hig01]), the poles typically have negative curvature, whereas the other vertices have positive or zero curvature. The example in Figure 2.2, as the minimal member of the $E^R_\square 1$ family, is an exception – the poles also have positive curvature. It is alternatively given by projecting the cube onto the sphere. The tilings given by projecting the Platonic solids onto the sphere are called the *Platonic tilings*.

The earth map tilings and the Platonic tilings can further give rise to variant tilings through subdivisions and *modifications* (flips and rotations [CLY22, CLY23]). The tilings not fitting into the above descriptions are called *sporadic*.

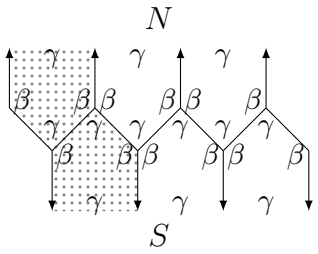

Figure 2.2: $E^R_\square 1$ with three time zones (one shaded by dots); $\uparrow$'s (resp. $\downarrow$'s) converge to N (resp. S); the leftmost and the rightmost boundaries are identified.

Similar to the Platonic tilings, one can obtain dihedral tilings by projecting the Archimedean solids onto the sphere [AHS18].

The tilings in the main theorem below are termed under an analogous convention. The infinite family of dihedral tilings are given by the all-rhombus time zones in the monohedral tilings $E^R_\square 1$ plus two squares; the other tilings, except for two, are structurally related to the cube, the snub cube, or the truncated octahedron. A structural relation not seen in monohedral tilings is explained by fusion – a reverse process of subdivision. We summarise the data of the tilings in Table 2.1 and give an account of their structures afterwards. The convexity of prototiles comes as a consequence of (3.7).

Theorem. *The edge-to-edge dihedral tilings of the sphere by the squares and the rhombi are of*

I. Earth map type: an infinite family of tilings each of which has $8c-2$ *tiles for* $c \geqslant 2$ *and among them* 2 *are squares and* $8c-4$ *are rhombi;*

II. Platonic type and Archimedean type:

- *one deformed cube with* 6 *tiles and among them* 2 *are squares and* 4 *are rhombi;*
- *two triangular fusions of the snub cube, each of which has* 22 *tiles and among them* 6 *are squares and* 16 *are rhombi;*
- *one quadrilateral subdivision of a deformed truncated octahedron with* 30 *tiles and among them* 6 *are squares and* 24 *are rhombi;*

III. Sporadic type: two tilings, each of which has 14 *tiles and among them* 10 *are squares and* 4 *are rhombi.*

In Table 2.1 as well as the later discussion, a vertex is represented by a *vertex notation* in terms of its incident angles counting multiplicities. For example, for non-negative integers a, b, c, a vertex notation $\alpha^a\beta^b\gamma^c$ denotes a vertex having a copies of α and b copies of β and c copies of γ as incident angles. Abusing notation, we call such a vertex "$\alpha^a\beta^b\gamma^c$". A concrete example is $\beta^2\gamma$ in Figure 2.2 where $a=0, b=2$ and $c=1$. In practice, we display only positive a, b, c whenever it is clear from the context. Note that the notation does not specify the angle arrangement at a vertex. By $k\alpha^a\beta^b\gamma^c$, we mean that there are exactly k such vertices in a tiling.

Tilings	Symmetry	#Vertices (Incident ∠s)	Angles & Edge	Prototiles	
				#□	#◊
Earth map type (Figure 2.3)	D_4	$8(c-1)\beta^2\gamma$, $8\alpha\beta\gamma^{c\geqslant 2}$	(4.14) for $c=2$ (4.15) for $c=3$	2	$8c-4$
Deformed cube (Figure 2.4a)	D_4	$8\alpha\beta\gamma$	$\alpha+\beta+\gamma=2\pi$	2	4
Triangular fusion of the snub cube (Figure 2.4b)	D_4	$8\alpha\beta^2$, $16\alpha\beta\gamma^2$	(4.4)	6	16
Triangular fusion of the snub cube (Figure 2.4c)	D_2	$8\alpha\beta^2$, $16\alpha\beta\gamma^2$	(4.4)	6	16
Quadrilateral subdivision of a truncated octahedron (Figure 2.4d)	C_4	$8\beta^3$, $32\alpha\beta\gamma^2$	(4.2)	6	24
Sporadic type (Figure 2.4e)	D_{4h}	$8\alpha^2\beta$, $8\alpha^3\gamma$	(4.6)	10	4
Sporadic type (Figure 2.4f)	1	$8\alpha^2\beta$, $8\alpha^3\gamma$	(4.6)	10	4

Table 2.1: Data of the tilings; □ denotes the square and ◊ denotes the rhombus.

The structures of the tilings are revealed by their plane drawings in Figures 2.3, 2.4, and their 3D images in Figure 2.5. Interactive 3D models are available at `https://www.geogebra.org/m/gk87uerw`. Further analysis is aided by Figures 2.6, 2.7, 2.8.

The infinite family of earth map type can be derived from the monohedral tilings $E^R_{\square}1$ in the following way. Figure 2.3a illustrates $\frac{3}{2}$ time zones of $E^R_{\square}1$ with γ^3 at the $*$-end and γ^2 at the $\star$-end. Let $\mathcal{T}$ denote the general version of $c-\frac{1}{2}$ time zones such that $\mathcal{T}$ consists of $2c-1$ rhombi with γ^c (resp. γ^{c-1}) at the $*$-end (resp. the $\star$-end). Then Figure 2.3a illustrates $\mathcal{T}$ for $c=3$. The dihedral tilings of earth map type are constructed by four copies of $\mathcal{T}$ and two squares. The four $\mathcal{T}$'s are glued together between the two squares as illustrated in Figure 2.3b. The two squares resemble the Arctic and Antarctic circles, whereas the $\mathcal{T}$'s resemble the continents and the rhombi resemble the countries. The plane drawing of the tiling with $c=2$ is fully illustrated in Figure 4.13. We remark that when $c=1$, the corresponding vertices become $\alpha\beta\gamma$ where $\alpha=\beta=\gamma$ and the tiling is monohedral given by the cube.

The plane drawings of the tilings of Platonic, Archimedean and sporadic types are illustrated in Figure 2.4: the (deformed) cube in Figure 2.4a, the two triangular fusions of the snub cube in Figures 2.4b and 2.4c, a quadrilateral subdivision of the hexagonal faces in a deformed truncated octahedron in Figure 2.4d, and the two sporadic tilings in Figures 2.4e and 2.4f.

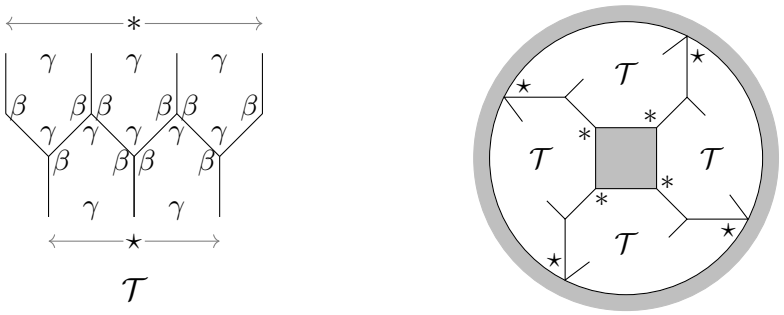

(a) $\mathcal{T}$ for $c = 3$. (b) Tiling: the square viewpoint.

Figure 2.3: The tilings of earth map type; $* = \gamma^c$ and $\star = \gamma^{c-1}$ for $c \geqslant 2$.

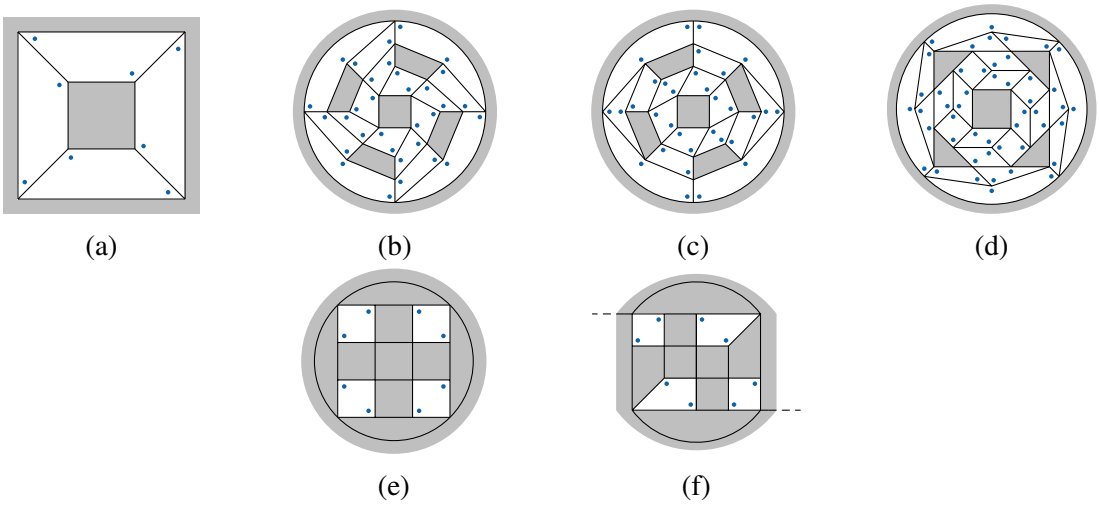

Figure 2.4: The four tilings of Platonic type and Archimedean type, and two sporadic tilings, where $\bullet = \beta$, and the dashed lines join to form one edge.

The two triangular fusions of the snub cube are explained in Figure 2.6. Figure 2.6a is given by the snub cube, a dihedral tiling of the sphere by regular triangles and squares. In general, if the triangles in a tiling can be grouped into adjacent pairs, then fusing the adjacent pairs results in quadrilateral tiles. In the snub cube, all the possible ways of grouping the triangles are shown in Figures 2.6b, 2.6c and 2.6d, where the dashed lines indicate the choices of adjacent pairs. As all the triangles are regular, the fusions yield congruent rhombi.

To distinguish the tilings, we label the vertices at the squares with exterior edge configuration "dashed-solid-solid" by •'s. The distribution of •'s distinguishes the tiling in Figure 2.6b (Figure 2.4b) and that in Figure 2.6c (Figure 2.4c). Guided by the distribution of •'s, it can be seen that Figure 2.6b and Figure 2.6d are mirror images: exterior edges incident to each • are counter-clockwise "solid-solid-dashed" in the former and "dashed-solid-solid" in the latter. There are indeed only two tilings resulting from the fusions.

Moreover, these two tilings are related, via a rotation modification as explained in Figure 2.7. In each tiling, we colour the boundaries of two octagonal disks, likewise in Figure 2.8. Each disk

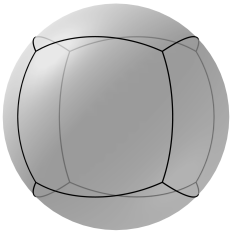

Figure 2.3b: $c = 1$

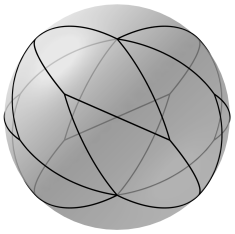

Figure 2.3b: $c = 2$

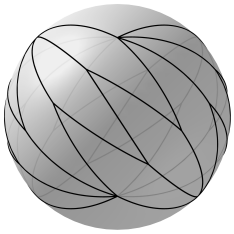

Figure 2.3b: $c = 3$

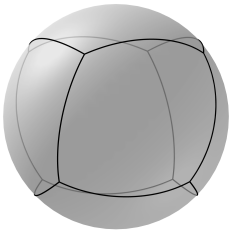

Figure 2.4a

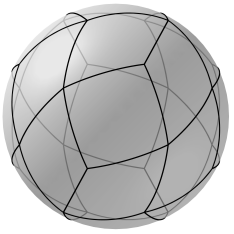

Figure 2.4b

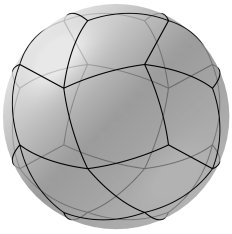

Figure 2.4c

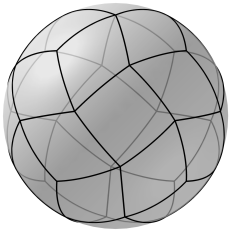

Figure 2.4d

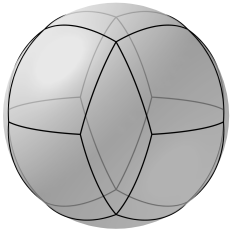

Figure 2.4e

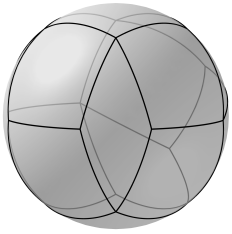

Figure 2.4f

Figure 2.5: The tilings from the main theorem in 3D.

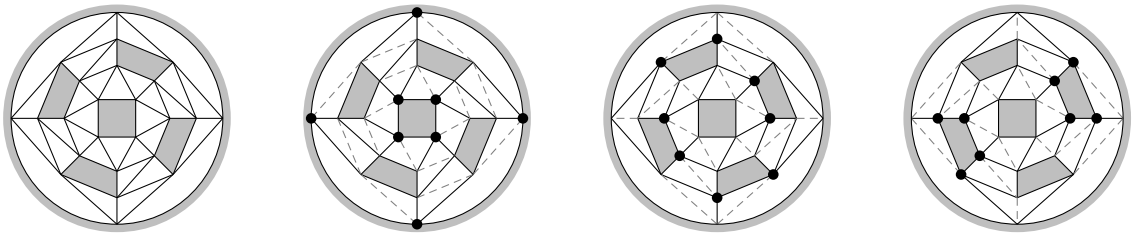

(a) (b) (c) (d)

Figure 2.6: Triangular fusions of the snub cube.

consists of a ring of six rhombi enclosing a square. Rotating the disk consisting of the outer ring of rhombi and the outer square in Figure 2.7a (Figure 2.6c) gives Figure 2.7b (Figure 2.6d) and vice versa. In Proposition 4.4, we show that a square with four •-vertices uniquely determines the tiling in Figure 2.6b.

The two sporadic tilings (Figures 2.4e, 2.4f) are also related, via a flip modification as explained in Figure 2.9. Each tiling can be divided into two hemispheres as highlighted. We rep-

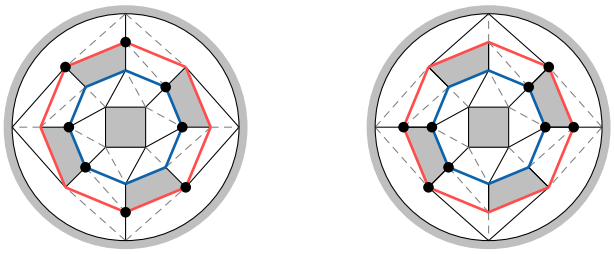

(a) Figure 2.6c. (b) Figure 2.6d.

Figure 2.7: A modification relating two triangular fusions of the snub cube.

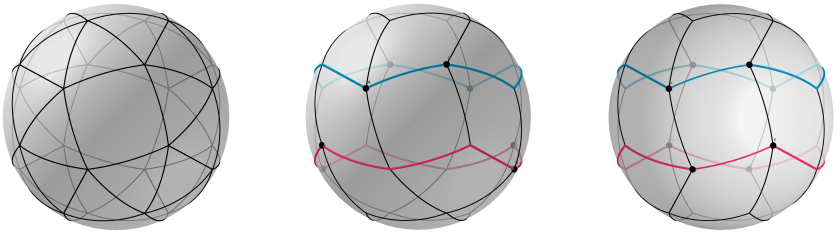

Spherical Snub Cube Figure 2.7a Figure 2.7b

Figure 2.8: Tilings in 3D, the snub cube and those given by triangular fusions.

resent the hemisphere containing the circled β as the outer disk in the second row of Figure 2.9 and the other hemisphere as the inner disk. An inner disk can be flipped along the dashed line to convert one tiling into another. It is easy to see using notations $\bullet = \beta$, $\circ = \alpha^2$, $\bullet = \alpha$, and $\circ = \alpha^2\gamma$ where angle values $\bullet + \circ = \bullet + \circ = 2\pi$. See also Figure 2.10 for comparison.

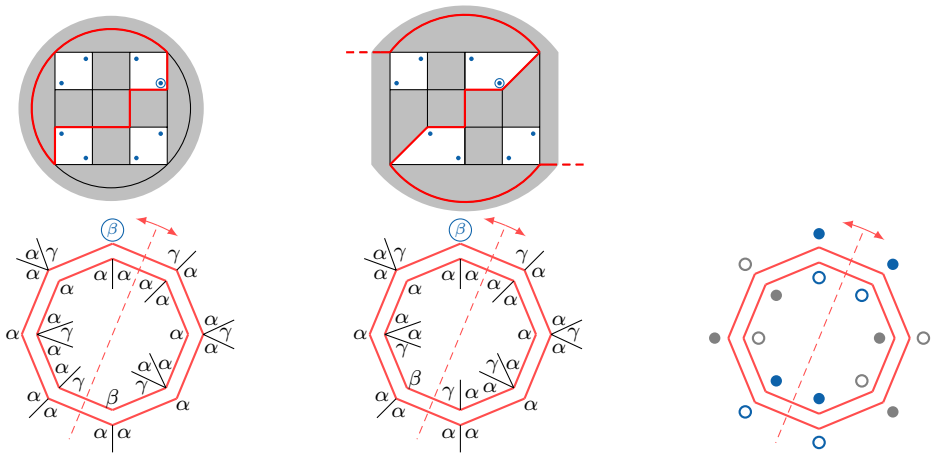

Figure 2.9: A modification relating two sporadic tilings; one hemisphere can be flipped along the dashed line, where $\bullet = \beta$, $\circ = \alpha^2$, $\bullet = \alpha$, and $\circ = \alpha^2\gamma$.

Notably, the tiling of earth map type with $c = 2$ in Figure 4.13b and the sporadic tiling in Figure 2.4e share the same underlying graph.

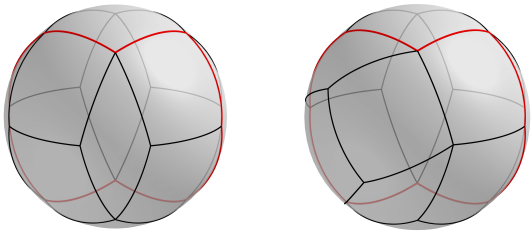

Before flip After flip

Figure 2.10: The sporadic tilings in 3D, the flip-related hemispheres have boundaries coloured.

The tiling in Figure 2.4d results from a quadrilateral subdivision of the hexagons in the slightly deformed truncated octahedron in Figure 2.11. Each hexagon is subdivided into 3 rhombi meeting at a β^3-vertex.

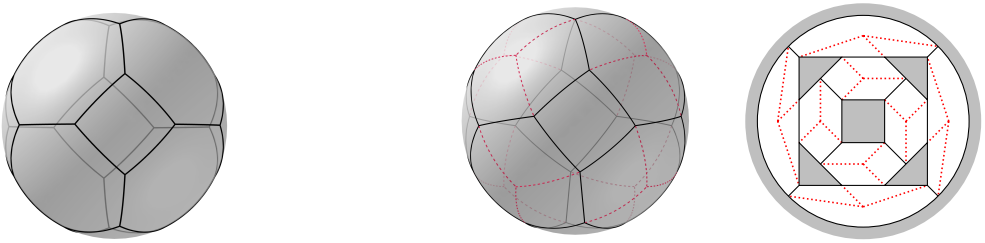

The truncated octahedron. A deformed truncated octahedron with subdivided hexagons.

Figure 2.11: Quadrilateral subdivision of the hexagons in a deformed truncated octahedron.

3. Toolbox

The "admissible" vertices of an associated tiling are consequences of the necessary conditions of the tiling. They determine locally how tiles can be put together. Knowing them allows us to step-by-step construct the tilings. Hence tools are built for this specific reason.

Starting with the basic combinatorial facts, let f denote the number of tiles and v_i denote the number of degree i vertices for $i \geqslant 3$. From [CLY22, (3.4), (3.5)] or [Nv14], we have

$$f = 6 + \sum_{h \geqslant 4} (h-3)v_h, \tag{3.1}$$

$$v_3 = 8 + \sum_{h \geqslant 4} (h-4)v_h. \tag{3.2}$$

Equation (3.2) implies that a tiling has a degree 3 vertex.

Recall from Section 2 that a vertex notation $\alpha^a\beta^b\gamma^c$ denotes a vertex by its incident angles counting multiplicities. The *vertex angle sum* of vertex $\alpha^a\beta^b\gamma^c$ gives the equation

$$a\alpha + b\beta + c\gamma = 2\pi. \tag{3.3}$$

Since vertex angle sums are used frequently enough in our discussion, they are often implicitly used without being mentioned.

A vertex with partial information on its incident angles can be denoted similarly by a vertex notation, where the known angles with multiplicities are followed by *the remainder* $\cdots$ of the vertex, and the value of the remainder is denoted by R. For example, $\alpha\beta^2\cdots$ denotes a vertex with at least one α and two β's, i.e., $a \geqslant 1$ and $b \geqslant 2$, and $R(\alpha\beta^2) = 2\pi - \alpha - 2\beta$.

Since a vertex notation does not specify how the angles are arranged, we use another system of notations for angle arrangements. For example, we use $\alpha_1\gamma_2\cdots$ to denote the vertex in Figure 3.1a where α from tile T_1 (displayed as ①) and γ from tile T_2 (②) are two incident angles. To emphasise α_1 being adjacent to γ_2 along an edge " | ", we use $\alpha_1|\gamma_2\cdots$ to denote such a vertex. The same picture shows that $\alpha|\gamma\cdots$ is a vertex if and only if $\alpha|\beta\cdots$ is a vertex. Similarly, T_1 and T_2 in Figure 3.1b show that $\beta|\beta\cdots$ is a vertex if and only if $\gamma|\gamma\cdots$ is also a vertex. The notations can be extended to a full vertex. For example, we use $|\alpha|\alpha|\alpha|$ to denote an angle arrangement of α^3 (Figure 3.1c).

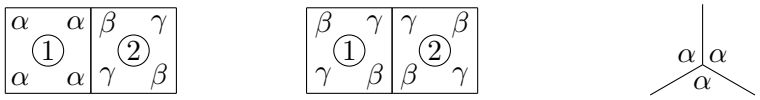

(a) (b) (c)

Figure 3.1: The angle arrangements of $\alpha|\gamma\cdots$, $\beta|\beta\cdots$, $\gamma|\gamma\cdots$ and α^3.

We first establish local properties in the next two lemmas.

Lemma 3.1. *In an edge-to-edge dihedral tiling by the squares and the rhombi, both $\alpha\beta\cdots$ and $\alpha\gamma\cdots$ are vertices.*

Proof. Since there is a square adjacent to a rhombus, the assertion follows from Figure 3.1a. □

The angle sum of a spherical quadrilateral is $> 2\pi$. For the square, we have $4\alpha > 2\pi$; and for the rhombus, we have $2\beta + 2\gamma > 2\pi$. They respectively imply

$$\alpha > \tfrac{1}{2}\pi, \tag{3.4}$$

$$\beta + \gamma > \pi. \tag{3.5}$$

Up to symmetry, we may assume $\beta > \gamma$.

Lemma 3.1 implies that one of $\alpha^a\beta^b, \alpha\beta\gamma\cdots$ is a vertex. Then one of the inequalities, $2\alpha + \beta \leqslant 2\pi$ and $\alpha + 2\beta \leqslant 2\pi$ and $\alpha + \beta + \gamma \leqslant 2\pi$, holds. Combined with $\alpha > \frac{1}{2}\pi$ and $\beta > \gamma$ and $\beta + \gamma > \pi$, we get $\alpha, \gamma < \pi$.

Lemma 3.2. *For the square with angle α and the rhombus with angles β, γ, if they have edges of the same length x, then we have*

$$\tan^2 \tfrac{1}{2}\alpha = \tan \tfrac{1}{2}\beta \tan \tfrac{1}{2}\gamma. \tag{3.6}$$

For $\beta > \gamma$, we also have

$$\pi > \beta > \alpha > \gamma. \tag{3.7}$$

The edge length x and the angles α, β, γ are related as follows,

$$\cos x = \cot^2 \tfrac{1}{2}\alpha = \cot \tfrac{1}{2}\beta \cot \tfrac{1}{2}\gamma. \tag{3.8}$$

Proof. By [Tod86, Art. 62] or [CLY22, Lemma 18], both sides of (3.6) is $\frac{1}{\cos x}$. By $\alpha, \gamma < \pi$, it implies $\tan \frac{1}{2}\beta > 0$, meaning $\beta < \pi$. Because of $\beta > \gamma$ and $\tan\theta$ being strictly increasing on $(0, \frac{1}{2}\pi)$, it further implies (3.7). □

From now on, we may assume $\beta > \alpha > \gamma$. Lemma 3.1 asserts that $\alpha\beta\cdots$ is a vertex. Its vertex angle sum implies

$$\alpha + \beta + \gamma \leqslant 2\pi. \tag{3.9}$$

We summarise the important inequalities (3.4), (3.5), (3.7), (3.9) below,

$$\alpha > \tfrac{1}{2}\pi, \quad \beta + \gamma > \pi > \beta > \alpha > \gamma, \quad \alpha + \beta + \gamma \leqslant 2\pi.$$

They will be frequently used without reference.

Next, a global property is stated below as an adaptation of [CLY22, Lemma 4].

Lemma 3.3 (Counting Lemma)**.** *In an edge-to-edge dihedral tiling of the sphere by the squares and the rhombi, if at every vertex the number of β is no more than the number of γ, then at every vertex the two numbers are equal.*

We remark that any of the notations for vertices, with full or partial incident angle information, can indeed be extended to represent a *vertex type*, i.e., the equivalence class of vertices having the same angle combination. For example, Lemma 3.1 implies that a tiling has a vertex of the types $\alpha\beta\cdots$ and a vertex of the type $\alpha\gamma\cdots$. Another example is (4.3) stated below,

$$\alpha\gamma\cdots = \alpha^3\gamma, \alpha^2\gamma^2, \alpha^2\gamma^3, \alpha\gamma^3, \alpha\gamma^4, \alpha\gamma^5, \alpha\beta\gamma^2,$$

which denotes a list of all possible vertex types for $\alpha\gamma\cdots$ in a tiling. It does not mean that every vertex type on the right-hand side appears as a vertex in the same tiling. A list of vertex types can indeed be refined recursively by the necessary conditions of a tiling.

In practice, the context mostly allows an abuse of notation without distinguishing between a vertex and a vertex type. In particular, a set of vertex types in a tiling satisfying the required conditions is called an *anglewise vertex combination* (abbreviated as AVC), which is what we meant by "admissible vertices" at the start of the section. An example is (4.8) stated below,

$$\mathrm{AVC} = \{\beta^2\gamma, \beta\gamma^c, \alpha\beta\gamma^c\}.$$

Note that the generic c may take different values at different vertices. The tilings constructed from (4.8) actually do not have $\beta\gamma^c$. For that and in general, we use "$\equiv$" in place of "$=$" to indicate that every vertex type in the set is indeed present as a vertex in a tiling. An example which gives the tilings in Figure 4.13 is (4.9) stated below,

$$\mathrm{AVC} \equiv \{\beta^2\gamma, \alpha\beta\gamma^c\}.$$

Obviously, the system of angle sum equations from the vertices in an AVC must be consistent.

4. Classification

From (3.2), we know that there is a degree 3 vertex in a tiling. Because of (3.7), (3.9), and $\alpha\beta\cdots$ being a vertex, we know that $\gamma^3, \alpha^2\gamma, \alpha\gamma^2, \beta\gamma^2$ are not vertices. Therefore, one of the following must appear as a degree 3 vertex,

$$\alpha^3, \beta^3, \alpha^2\beta, \alpha\beta^2, \beta^2\gamma, \alpha\beta\gamma.$$

They are studied in the following propositions. Some arguments may be simplified in terms of constraint satisfaction problems aided by computer. Nevertheless, here we prioritise mathematical rigour and clarity.

Proposition 4.1. *There is no edge-to-edge dihedral tiling of the sphere by the squares and the rhombi with a vertex α^3.*

Proof. For $\beta^2\cdots$, the inequality $\beta+\gamma > \pi$ implies $R(\beta^2) = 2\pi - 2\beta < 2\gamma$. Assume that α^3 is a vertex. Then its vertex angle sum $3\alpha = 2\pi$ and $\beta > \alpha$ imply $R(\beta^2) < \alpha$. Hence $R(\beta^2) < \alpha, 2\gamma$ determines $\beta^2\cdots = \beta^2\gamma$.

Suppose that both $\alpha^3, \beta^2\gamma$ are vertices. Their vertex angle sums imply

$$\alpha = \tfrac{2}{3}\pi, \quad \beta = \pi - \tfrac{1}{2}\gamma.$$

Substituting the above into (3.6) further gives

$$3 = \cot\tfrac{1}{4}\gamma \tan\tfrac{1}{2}\gamma = \frac{2}{1-\tan^2\frac{1}{4}\gamma},$$

which implies $\gamma = \frac{2}{3}\pi = \alpha$, a contradiction. Hence $\beta^2\gamma$ is not a vertex and therefore $\beta^2\cdots$ is not a vertex.

The absence of $\beta^2\cdots$ and $\beta > \alpha = \frac{2}{3}\pi > \gamma$ imply $\beta\cdots = \beta\gamma^c, \alpha\beta\gamma^c$. Counting Lemma (Lemma 3.3) further implies $\beta\cdots = \alpha\beta\gamma$ and hence $\gamma\cdots = \alpha\beta\gamma$. Therefore the admissible vertices are given by

$$\mathrm{AVC} = \{\alpha^3, \alpha\beta\gamma\}. \tag{4.1}$$

From the above, we know $\alpha^2\cdots = \alpha^3$, applying which at the neighbours of an α^3 repeatedly determines a monohedral tiling in Figure 4.1a. This means that there is no dihedral tiling. □

Proposition 4.2. *The edge-to-edge dihedral tiling of the sphere by the squares and the rhombi with a vertex $\alpha\beta\gamma$ is given by a deformed cube.*

The tiling has 2 squares and 4 rhombi (see Figures 2.4a, 4.1b).

Proof. The vertex angle sum of $\alpha\beta\gamma$ and $\beta > \alpha > \gamma$ imply $R(\beta^2) < R(\alpha\beta) = \gamma$. Then $\beta^2\cdots$ is not a vertex and $\alpha\beta\cdots = \alpha\beta\gamma$. Hence $\beta\cdots = \alpha\beta\gamma, \beta\gamma^c$. Then by Counting Lemma, we conclude $\beta\cdots = \gamma\cdots = \alpha\beta\gamma$, applying which at the neighbours of an $\alpha\beta\gamma$ repeatedly determines the desired tiling. □

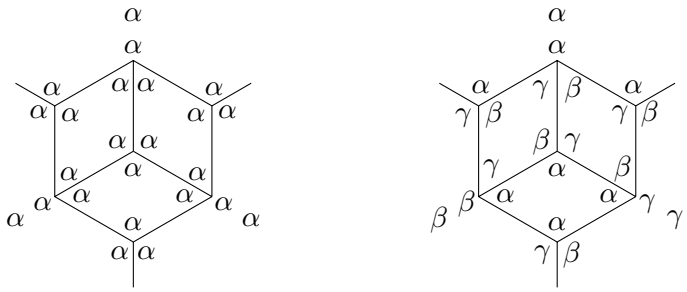

(a) Monohedral. (b) Dihedral.

Figure 4.1: The monohedral tiling with α^3 and the dihedral tiling with $\alpha\beta\gamma$.

Proposition 4.3. *The edge-to-edge dihedral tiling of the sphere by the squares and the rhombi with a vertex β^3 is given by a quadrilateral subdivision of a deformed truncated octahedron.*

The tiling has 6 squares and 24 rhombi (see Figure 2.4d).

Proof. The vertex angle sum of β^3 implies $\beta = \frac{2}{3}\pi$. Then $\beta > \alpha > \gamma$ and $\beta + \gamma > \pi$ imply $2\gamma > \beta > \alpha > \gamma > \frac{1}{3}\pi$ and hence $\beta^2\cdots = \beta^3$.

Lemma 3.1 asserts that $\alpha\beta\cdots$ is a vertex. Then $\alpha > \frac{1}{2}\pi$ and $\beta = \frac{2}{3}\pi$ and $\gamma > \frac{1}{3}\pi$ imply $R(\alpha\beta) < \frac{5}{6}\pi < \alpha+\gamma, 3\gamma$. As $\beta^2\cdots = \beta^3$, it then implies $\alpha\beta\cdots = \alpha\beta\gamma^2$ and hence $\alpha\beta\gamma^2$ is also a vertex. Together with $2\gamma > \beta > \alpha$, it implies $\beta\gamma^2\cdots = \alpha\beta\gamma^2$.

Keeping in mind $\beta^2\cdots = \beta^3$ and $\alpha\beta\cdots = \beta\gamma^2\cdots = \alpha\beta\gamma^2$, we construct the tiling as follows. At square T_1 and rhombus T_2 in Figure 4.2, $\alpha_1\beta_2\cdots = \alpha\beta\gamma^2$ determines T_3, T_4. Then $\alpha_1\beta_4\cdots = \alpha\beta\gamma^2$ determines T_5, T_6. The same argument determines T_7, T_8, T_9. Next, $\beta_3\beta_4\cdots = \beta^3$ determines T_{10}, and $\beta_5\gamma_4\gamma_{10}\cdots = \alpha\beta\gamma^2$ further determines T_{11}, and $\alpha_{11}\beta_{10}\cdots = \alpha\beta\gamma^2$ determines T_{12}, T_{13}. By rotational symmetry, the same argument determines $T_{14}, T_{15}, T_{16}, T_{17}$, and $T_{18}, T_{19}, T_{20}, T_{21}$, and $T_{22}, T_{23}, T_{24}, T_{25}$. Next, $\alpha_{11}\beta_{13}\gamma_{16}\cdots = \alpha\beta\gamma^2$ determines T_{26}. Again by rotational symmetry, the same argument determines T_{27}, T_{28}, T_{29}. Finally, $\beta_{26}\gamma_{13}\gamma_{29}\cdots = \alpha\beta\gamma^2$ determines T_{30} and hence the tiling.

The tiling has AVC $\equiv \{\beta^3, \alpha\beta\gamma^2\}$. The vertex angle sums and (3.8) give

$$\alpha = (0.53584\ldots)\pi, \quad \beta = \tfrac{2}{3}\pi, \quad \gamma = (0.39874\ldots)\pi, \quad x = (0.20591\ldots)\pi. \tag{4.2}$$

□

Proposition 4.4. *The edge-to-edge dihedral tilings of the sphere by the squares and the rhombi with a vertex $\alpha\beta^2$ are given by two triangular fusions of the snub cube.*

Each tiling has 6 squares and 16 rhombi (see Figures 2.4b, 2.4c, or Figures 4.6a, 4.6b).

Proof. The vertex angle sum of $\alpha\beta^2$ and $\beta > \alpha > \frac{1}{2}\pi$ imply $\frac{3}{4}\pi > \beta > \frac{2}{3}\pi > \alpha$. Then $\beta+\gamma > \pi$ and $\alpha\beta^2$ imply $2\gamma > \alpha$, which further deduces $\gamma > \frac{1}{4}\pi$ and $3\gamma > \frac{3}{4}\pi > \beta$. Moreover, $\alpha > \frac{1}{2}\pi$ and $\gamma > \frac{1}{4}\pi$ and $\frac{3}{4}\pi > \beta$ imply $\alpha + \gamma > \beta$. To sum up, we have $\alpha+\gamma, 3\gamma > \beta > \alpha > \gamma$.

Furthermore, the vertex angle sum of $\alpha\beta^2$ also implies $\gamma < \alpha < R(\alpha\beta) = \beta < \alpha+\gamma, 3\gamma$, and hence $\alpha\beta\cdots = \alpha\beta^2, \alpha\beta\gamma^2$. Similarly, $\gamma < R(\beta^2) = \alpha < \beta, 2\gamma$ imply $\beta^2\cdots = \alpha\beta^2$.

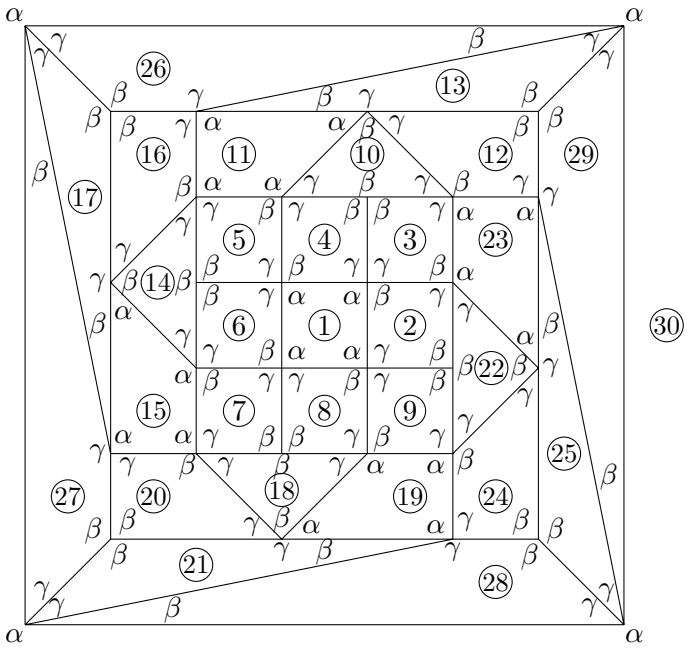

Figure 4.2: The construction of the tiling with a vertex β^3.

Lemma 3.1 asserts that $\alpha\gamma\cdots$ is a vertex. To determine $\alpha\gamma\cdots$, we use $\alpha > \frac{1}{2}\pi$ and $\gamma > \frac{1}{4}\pi$ and $\alpha\beta\cdots = \alpha\beta^2, \alpha\beta\gamma^2$ and obtain

$$\alpha\gamma\cdots = \alpha^3\gamma, \alpha^2\gamma^2, \alpha^2\gamma^3, \alpha\gamma^3, \alpha\gamma^4, \alpha\gamma^5, \alpha\beta\gamma^2. \tag{4.3}$$

The above then implies $\alpha^2\gamma\cdots = \alpha^3\gamma, \alpha^2\gamma^2, \alpha^2\gamma^3$.

By $2\gamma > \alpha > \gamma$, we also know $\alpha \neq k\gamma$ and $\alpha \neq \frac{1}{k}\gamma$ for $k \in \mathbb{N}$.

Keeping in mind $\alpha\beta\cdots = \alpha\beta^2, \alpha\beta\gamma^2$ and $\beta^2\cdots = \alpha\beta^2$, we analyse the cases below.

Case (One of $\alpha\gamma^3, \alpha\gamma^4, \alpha\gamma^5$). The vertex angle sum given by one of $\alpha\gamma^3, \alpha\gamma^5$ and the vertex angle sum by one of $\alpha^3\gamma, \alpha^2\gamma^2, \alpha^2\gamma^3$ (vertices of type $\alpha^2\gamma\cdots$) imply $\alpha = k\gamma$ where $k = 0, 1, 2$ or 3, a contradiction. The same contradiction is also given by $\alpha\gamma^4$ and one of $\alpha^2\gamma^2, \alpha^2\gamma^3$. Hence any of $\alpha\gamma^3, \alpha\gamma^5$ and $\alpha^2\gamma\cdots$ are mutually exclusive, while $\alpha\gamma^4$ implies $\alpha^2\gamma\cdots = \alpha^3\gamma$.

The angle arrangement of $\alpha\gamma^3, \alpha\gamma^4$ or $\alpha\gamma^5$ has a $\gamma|\gamma|\gamma$, which determines tiles T_1, T_2, T_3 in Figure 4.3a. Then $\beta_1\beta_2\cdots, \beta_2\beta_3\cdots = \alpha\beta^2$ respectively determine T_4, T_5. Now $\alpha_4\alpha_5\gamma_2\cdots$ (as $\alpha^2\gamma\cdots$) rules out $\alpha\gamma^3, \alpha\gamma^5$ and hence $\alpha\gamma^4, \alpha^3\gamma$ are both vertices.

The vertex angle sums of $\alpha\beta^2, \alpha\gamma^4, \alpha^3\gamma$ imply

$$\alpha = \tfrac{6}{11}\pi, \quad \beta = \tfrac{8}{11}\pi, \quad \gamma = \tfrac{4}{11}\pi,$$

which fail (3.6). Therefore none of $\alpha\gamma^3, \alpha\gamma^4, \alpha\gamma^5$ is a vertex.

Case (One of $\alpha^2\gamma^2, \alpha^2\gamma^3$). The vertex angle sums of $\alpha\beta\gamma^2$ and one of $\alpha^2\gamma^2, \alpha^2\gamma^3$ imply $\alpha = \beta$ and $\alpha + \gamma = \beta$ respectively; the former contradicts $\beta > \alpha$ while the latter contradicts $\alpha + \gamma > \beta$. Hence $\alpha\beta\gamma^2$ is not a vertex and $\alpha\beta\cdots = \alpha\beta^2$.

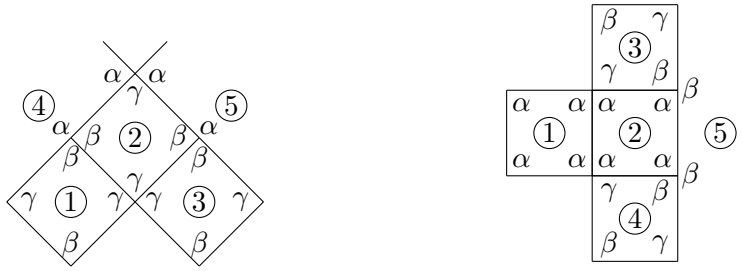

(a) $\gamma|\gamma|\gamma$ and $\alpha|\gamma|\alpha$ (b) $\alpha|\alpha$

Figure 4.3: The deductions from $\gamma|\gamma|\gamma$ and $\alpha|\gamma|\alpha$ and $\alpha|\alpha$.

The angle arrangement $\alpha|\alpha$ determines tiles T_1, T_2 in Figure 4.3b. Up to mirror symmetry, by $\alpha^2\cdots = \alpha^2\gamma^c$ we determine T_3, T_4. Then $\alpha_2\beta_3\cdots, \alpha_2\beta_4\cdots = \alpha\beta^2$ give two adjacent β's in T_5, a contradiction. Hence $\alpha|\alpha\cdots$ is not a vertex and $\alpha^2\gamma^2, \alpha^2\gamma^3$ have $\alpha|\gamma|\alpha$ in their angle arrangements.

We reverse the deduction in Figure 4.3a. The angle arrangement $\alpha|\gamma|\alpha$ determines tiles T_4, T_2, T_5. Then $\alpha_4\beta_2\cdots, \alpha_5\beta_2\cdots = \alpha\beta^2$ determine the angles in T_1, T_3. Now T_1, T_2, T_3 meet at $\gamma_1|\gamma_2|\gamma_3\cdots$ and hence $\gamma|\gamma|\gamma\cdots$ is a vertex.

To determine $\gamma|\gamma|\gamma\cdots$, the absence of $\alpha|\alpha\cdots$ means $\gamma|\gamma|\gamma\cdots \neq \alpha^2\gamma^3$. The previous case has already ruled out $\alpha\gamma^3, \alpha\gamma^4, \alpha\gamma^5$. Then $\gamma|\gamma|\gamma\cdots$ is none of those in (4.3) and hence it has no α. Meanwhile, $2\gamma > \alpha$ and $3\gamma > \beta$ and $\alpha\beta^2$ imply $\beta\gamma^{c\geqslant 3} = \beta\gamma^3, \beta\gamma^4$. On the other hand, by $\frac{2}{3}\pi > \gamma > \frac{1}{4}\pi$ we get $\gamma^c = \gamma^4, \gamma^5, \gamma^6, \gamma^7$. Therefore $\gamma|\gamma|\gamma\cdots = \gamma^4, \gamma^5, \gamma^6, \gamma^7, \beta\gamma^3, \beta\gamma^4$.

Keep in mind that $\alpha\beta^2$ comes from the hypothesis; one of $\alpha^2\gamma^2, \alpha^2\gamma^3$ comes from the case assumption, which implies that one of $\gamma^4, \gamma^5, \gamma^6, \gamma^7, \beta\gamma^3, \beta\gamma^4$ is also a vertex.

The vertex angle sums of $\alpha^2\gamma^2$ and one of γ^4, γ^6 imply $\alpha = k\gamma$ for $k = 1, 2$ respectively, a contradiction. Similarly, $\alpha^2\gamma^2, \gamma^7$ imply $\alpha > 2\gamma$, also a contradiction. On the other hand, $\alpha\beta^2, \alpha^2\gamma^2, \beta\gamma^4$ imply $\alpha = \beta$, again a contradiction. Meanwhile, $\alpha\beta^2, \alpha^2\gamma^2$ and one of $\gamma^5, \beta\gamma^3$ imply

$$\begin{aligned} &\alpha\beta^2, \alpha^2\gamma^2, \gamma^5: && \alpha = \tfrac{3}{5}\pi, && \beta = \tfrac{7}{10}\pi, && \gamma = \tfrac{2}{5}\pi;\\ &\alpha\beta^2, \alpha^2\gamma^2, \beta\gamma^3: && \alpha = \tfrac{4}{7}\pi, && \beta = \tfrac{5}{7}\pi, && \gamma = \tfrac{3}{7}\pi. \end{aligned}$$

Both sets of angle values fail (3.6). Therefore $\alpha^2\gamma^2$ is not a vertex.

The vertex angle sums of $\alpha^2\gamma^3$ and one of $\gamma^4, \gamma^5, \gamma^7$ imply $\alpha = k\gamma$ for $k = \frac{1}{2}, 1, 2$ respectively, a contradiction. Similarly, $\alpha^2\gamma^3, \beta\gamma^3$ imply $\beta = 2\alpha > \pi$, also a contradiction. On the other hand, $\alpha\beta^2, \alpha^2\gamma^3, \gamma^6$ imply $\alpha = \frac{1}{2}\pi$, again a contradiction. Meanwhile, $\alpha\beta^2, \alpha^2\gamma^3, \beta\gamma^4$ imply

$$\alpha\beta^2, \alpha^2\gamma^3, \beta\gamma^4: \qquad \alpha = \tfrac{10}{19}\pi, \qquad \beta = \tfrac{14}{19}\pi, \qquad \gamma = \tfrac{6}{19}\pi,$$

which fail (3.6). Therefore $\alpha^2\gamma^3$ is also not a vertex.

Case ($\alpha^3\gamma$). Based on the previous cases, (4.3) is reduced to

$$\alpha\gamma\cdots = \alpha^3\gamma, \alpha\beta\gamma^2.$$

The vertex angle sums of $\alpha^3\gamma, \alpha\beta\gamma^2, \alpha\beta^2$ give the same angle values given by $\alpha\beta^2, \alpha\gamma^4, \alpha^3\gamma$, which we have already seen fail (3.6). Hence $\alpha\beta\gamma^2$ is not a vertex and therefore $\alpha\beta\cdots = \alpha\beta^2$.

For $\alpha|\gamma|\alpha$ in $\alpha^3\gamma$, the same reverse deduction in Figure 4.3a implies $\gamma|\gamma|\gamma\cdots$, meaning that it is a vertex. The reduced list of (4.3) above implies that $\gamma|\gamma|\gamma\cdots$ has no α. Moreover, the inequalities $2\gamma, \beta > \alpha > \gamma$ and the vertex angle sums of $\alpha\beta^2, \alpha^3\gamma$ further imply that $\gamma|\gamma|\gamma\cdots$ is one of $\gamma^5, \gamma^6, \beta\gamma^3, \beta\gamma^4$. Hence one of them is a vertex, together with $\alpha\beta^2, \alpha^3\gamma$, their vertex angle sums imply

$$\begin{aligned}
&\alpha\beta^2, \alpha^3\gamma, \gamma^5: && \alpha = \tfrac{8}{15}\pi, && \beta = \tfrac{11}{15}\pi, && \gamma = \tfrac{2}{5}\pi;\\
&\alpha\beta^2, \alpha^3\gamma, \gamma^6: && \alpha = \tfrac{5}{9}\pi, && \beta = \tfrac{13}{18}\pi, && \gamma = \tfrac{1}{3}\pi;\\
&\alpha\beta^2, \alpha^3\gamma, \beta\gamma^3: && \alpha = \tfrac{10}{19}\pi, && \beta = \tfrac{14}{19}\pi, && \gamma = \tfrac{8}{19}\pi;\\
&\alpha\beta^2, \alpha^3\gamma, \beta\gamma^4: && \alpha = \tfrac{14}{25}\pi, && \beta = \tfrac{18}{25}\pi, && \gamma = \tfrac{8}{25}\pi.
\end{aligned}$$

Each set of angle values above fail (3.6). Therefore $\alpha^3\gamma$ is not a vertex.

Case ($\alpha\beta\gamma^2$). By the previous cases, (4.3) becomes $\alpha\gamma\cdots = \alpha\beta\gamma^2$, and we already know up front $\alpha\beta\cdots = \alpha\beta^2, \alpha\beta\gamma^2$. The vertex angle sum of $\alpha\beta\gamma^2$ and $2\gamma > \alpha > \gamma$ rule out $\beta\gamma^{c\geqslant 2}$. Combined with $\beta^2\cdots = \alpha\beta^2$, we conclude $\beta\cdots = \alpha\beta^2, \alpha\beta\gamma^2$. By Proposition 4.1, we also conclude $\alpha\cdots = \alpha\beta^2, \alpha\beta\gamma^2$.

The vertex angle sums of $\alpha\beta^2, \alpha\beta\gamma^2$ imply

$$\beta = \pi - \tfrac{1}{2}\alpha, \quad \gamma = \tfrac{1}{2}\pi - \tfrac{1}{4}\alpha.$$

The above and (3.8) determine

$$\alpha = (0.55137\ldots)\pi, \quad \beta = (0.72431\ldots)\pi, \quad \gamma = (0.36215\ldots)\pi, \quad x = (0.24272\ldots)\pi. \tag{4.4}$$

Hence γ^c is not a vertex and $\gamma\cdots = \alpha\beta^2, \alpha\beta\gamma^2$. Therefore we get

$$\mathrm{AVC} = \{\alpha\beta^2, \alpha\beta\gamma^2\}. \tag{4.5}$$

Recall a fact from Figure 3.1b: $\beta|\beta\cdots$ is a vertex if and only if $\gamma|\gamma\cdots$ is a vertex. We know $\alpha\beta^2 = |\alpha|\beta|\beta|$ and from (4.5) we also know $\gamma|\gamma\cdots = |\alpha|\beta|\gamma|\gamma|$. Then there is an $\alpha\beta\gamma^2$ with angle arrangement $|\alpha|\beta|\gamma|\gamma|$. Denoting $|\alpha|\beta|\gamma|\gamma|$ by "•", there is a square with at least one •.

We first consider a square with a diagonal pair of •'s. If they are arranged as in Figure 4.4a, then they determine tiles T_1, T_2, T_3, T_4, T_5. Next, $\beta_2\beta_3\cdots, \beta_4\beta_5\cdots = \alpha\beta^2$ determine T_6, T_7, contradicting $\gamma_3\gamma_4\cdots = \alpha\beta\gamma^2$. Hence, if a square has a pair of diagonal •'s, then their angles must be arranged with the same orientation depicted in Figure 4.4b. This forces the other two vertices at the square to be •'s (indicated by •'s) as well. Hence a square with two diagonal •'s in fact has four •'s.

The above further implies that there are three possible distributions of •'s at a square, four •'s, two adjacent •'s, and exactly one •. Figure 4.5a illustrates the first as given by Figure 4.4b, and Figures 4.5b, 4.5c illustrate the latter two. A similar argument uniquely determines the angle

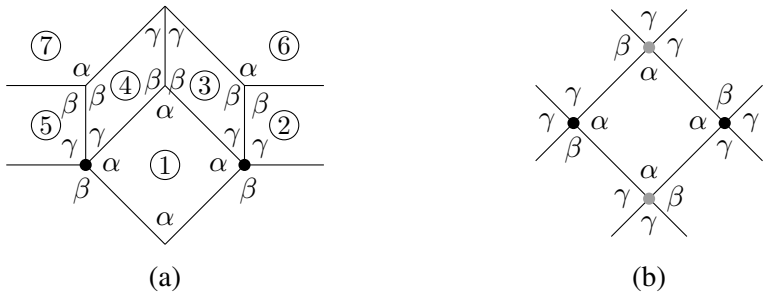

(a) (b)

Figure 4.4: Deductions from diagonal •'s at a square, where • $= |\alpha|\beta|\gamma|\gamma|$.

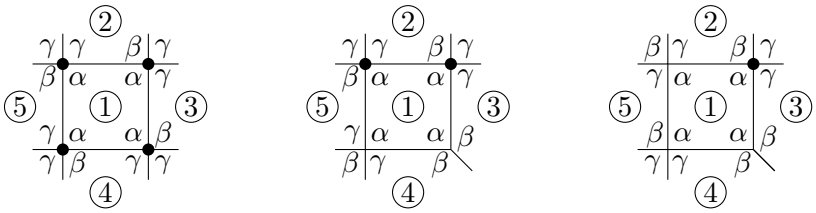

(a) (b) (c)

Figure 4.5: Distributions of $|\alpha|\beta|\gamma|\gamma|$'s at a square, where • $= |\alpha|\beta|\gamma|\gamma|$.

arrangements of $T_1, T_2, \ldots, T_5$ in these pictures. In Figure 4.5c, $\alpha_1\beta_5\gamma_4\cdots = |\alpha|\beta|\gamma|\gamma|$ turns it into Figure 4.4a, giving a contradiction as shown before.

As a result, a square with a • in a tiling has either the angle arrangement in Figure 4.5a or that in Figure 4.5b. If T_1 is given by the former (resp. the latter), then it uniquely determines the tiling in Figure 4.6a (resp. Figure 4.6b). Note that, Figure 4.6b shows the same tiling in Figure 2.4c from a different perspective.

(a) (b)

Figure 4.6: The two tilings with AVC $\equiv \{\alpha\beta^2, \alpha\beta\gamma^2\}$, where • $= |\alpha|\beta|\gamma|\gamma|$.

In the two tilings, dividing each rhombus (Figure 4.7a) into two regular triangles (because of $\beta = 2\gamma$) along the diagonal between two β's results in the same tiling in Figure 4.7b, a tiling given by the snub cube and $\alpha\gamma^4$ is the only vertex type. The reverse process gives the fusions.

Proposition 4.5. *The edge-to-edge dihedral tilings of the sphere by the squares and the rhombi with a vertex $\alpha^2\beta$ are the two sporadic tilings.*

Each tiling has 10 squares and 4 rhombi (see Figures 2.4e, 2.4f, 4.10).

(a) Dividing a rhombus into 2 triangles. (b) The snub cube.

Figure 4.7: A rhombus as the union of an adjacent pair of regular triangles in the snub cube. □

Proof. The vertex angle sum of $\alpha^2\beta$ and $\beta > \alpha$ imply $\beta > \frac{2}{3}\pi > \alpha$ and $R(\beta^2) < \alpha$. Meanwhile, $\beta + \gamma > \pi$ implies $R(\beta^2) < 2\gamma$. Then $\beta > \alpha > \gamma$ imply $\beta^2\cdots = \beta^2\gamma$.

The vertex angle sums of $\alpha^2\beta, \beta^2\gamma$ imply

$$\beta = 2\pi - 2\alpha, \quad \gamma = 4\alpha - 2\pi.$$

The above and (3.6) further imply

$$\tan^2 \tfrac{1}{2}\alpha = -\tan\alpha \tan 2\alpha.$$

Multiplying both sides by $\frac{(1+\cos\alpha)(2\cos^2\alpha-1)}{(1-\cos\alpha)}$ gives

$$(2\cos\alpha + 1)^2 = 0,$$

which has no solution for $\alpha \in (\frac{1}{2}\pi, \frac{2}{3}\pi)$. Hence $\beta^2\gamma$ is not a vertex and therefore the same for $\beta^2\cdots$. Propositions 4.1, 4.2, 4.3, 4.4 imply that $\alpha^2\beta$ is the only degree 3 vertex type.

Because of $\beta > \frac{2}{3}\pi > \alpha > \frac{1}{2}\pi$, the possible vertex types are

$$\alpha^2\beta, \gamma^c, \alpha^{a\leqslant 3}\gamma^c, \beta\gamma^c, \alpha\beta\gamma^c.$$

The absence of $\beta^2\cdots$ rules out $\beta|\beta\cdots$ as well as $\gamma|\gamma\cdots$ (see Figure 3.1b). The absence of $\gamma|\gamma\cdots$ means that $\gamma^c, \alpha\gamma^c, \beta\gamma^c$ are not vertices. Moreover, combined with $\alpha^2\beta$ being the only degree 3 vertex type, it implies $1 \leqslant c \leqslant 3$ in $\alpha^3\gamma^c$, and $c = 2$ in $\alpha^2\gamma^c, \alpha\beta\gamma^c$, and $\alpha|\beta\cdots = \alpha^2\beta$. It suffices to discuss

$$\alpha^2\beta, \alpha^3\gamma, \alpha^3\gamma^2, \alpha^3\gamma^3, \alpha^2\gamma^2, \alpha\beta\gamma^2.$$

Assume that one of $\alpha^2\gamma^2, \alpha\beta\gamma^2, \alpha^3\gamma^2, \alpha^3\gamma^3$ is a vertex. The absence of $\gamma|\gamma\cdots$ implies that the vertex has $\gamma|\alpha|\gamma$, which determines tiles T_1, T_2, T_3 in Figure 4.8. Then the absence of $\gamma|\gamma\cdots$ implies $\alpha_2|\beta_1\cdots, \alpha_2|\beta_3\cdots = \alpha^2\beta$, which further determine T_4, T_5. It results in $\alpha_4|\alpha_2|\alpha_5\cdots$, meaning that $\alpha^3\gamma$ is also a vertex.

The vertex angle sums of $\alpha^2\beta, \alpha^3\gamma$ and (3.8) determine α, β, γ, x below,

$$\alpha = 4\tan^{-1}\sqrt{\tfrac{1}{5}(11-4\sqrt{6})}, \quad \beta = 2\pi - 2\alpha, \quad \gamma = 2\pi - 3\alpha, \quad x = \cos^{-1}\tfrac{3}{5}. \tag{4.6}$$

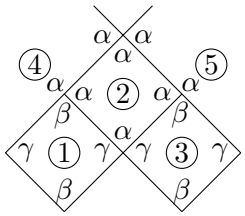

Figure 4.8: The deduction from $\gamma|\alpha|\gamma$.

Approximated values of the angles are given as follows,

$$\alpha = (0.58043\ldots)\pi, \quad \beta = (0.83913\ldots)\pi, \quad \gamma = (0.25870\ldots)\pi,$$

which contradict $\alpha^2\gamma^2, \alpha\beta\gamma^2, \alpha^3\gamma^2, \alpha^3\gamma^3$, and hence none of them is a vertex. We conclude

$$\mathrm{AVC} = \{\alpha^2\beta, \alpha^3\gamma\}. \tag{4.7}$$

From the above, we know $\beta\cdots = \alpha^2\beta$ and $\gamma\cdots = \alpha^3\gamma$.

The angle arrangement of $\alpha^3\gamma$ determines tiles T_1, T_2, T_3 in Figure 4.9. We know that $\alpha_1\alpha_2\cdots$ is $\alpha^2\beta$ or $\alpha^3\gamma$. If the undetermined $\alpha_1\alpha_2\cdots$ is $\alpha^2\beta$, then it determines T_5 in Figure 4.9a. Subsequently $\alpha_2\gamma_5\cdots = \alpha^3\gamma$ determines T_4. If the undetermined $\alpha_1\alpha_2\cdots$ is $\alpha^3\gamma$ as configured in Figure 4.9b, then it determines T_5, and $\alpha_2\beta_5\cdots = \alpha^2\beta$ determines T_4. We further get the undetermined $\alpha_2\alpha_3\cdots = \alpha_2\alpha_3\alpha_4\cdots = \alpha^3\gamma$. If the undetermined $\alpha_1\alpha_2\cdots = \alpha^3\gamma$ is otherwise configured, then a flip gives T_1, T_2, T_3, T_4 in Figure 4.9a. In either situation, we always have a "T-piece" formed by four squares T_1, T_2, T_3, T_4.

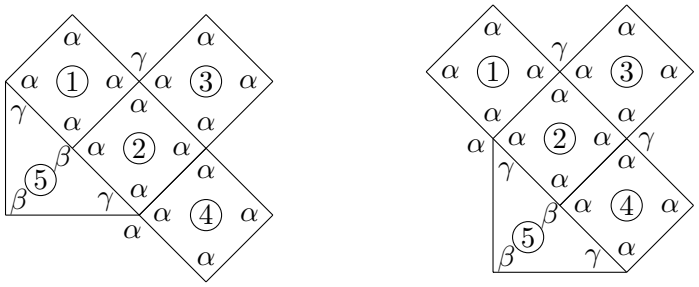

(a) (b)

Figure 4.9: The T-pieces in the deductions from $\alpha^3\gamma$.

For a T-piece with T_1, T_2, T_3, T_4 in Figure 4.9, it is either a square or a rhombus for the adjacent tile along the remaining undetermined edge of T_2.

If it is a square T_5 adjacent to T_2 in Figure 4.10a, then $\alpha_1\alpha_2\alpha_3\cdots$, $\alpha_1\alpha_2\alpha_5\cdots$, $\alpha_2\alpha_4\alpha_5\cdots$, and $\alpha_2\alpha_3\alpha_4\cdots = \alpha^3\gamma$ determine T_6, T_7, T_8, T_9 respectively. Now, $\alpha_1\beta_6\cdots = \alpha^2\beta$ further determines T_{10}. By rotational symmetry, a similar argument determines T_{11}, T_{12}, T_{13}. Finally, by $\alpha_{10}\alpha_{13}\gamma_6\cdots = \alpha^3\gamma$ we determine T_{14} and hence a tiling with 10 squares and 4 rhombi.

If it is a rhombus T_5 adjacent to T_2 in Figure 4.10b, then a similar argument determines another tiling with the same vertex types and the same number of tiles. □

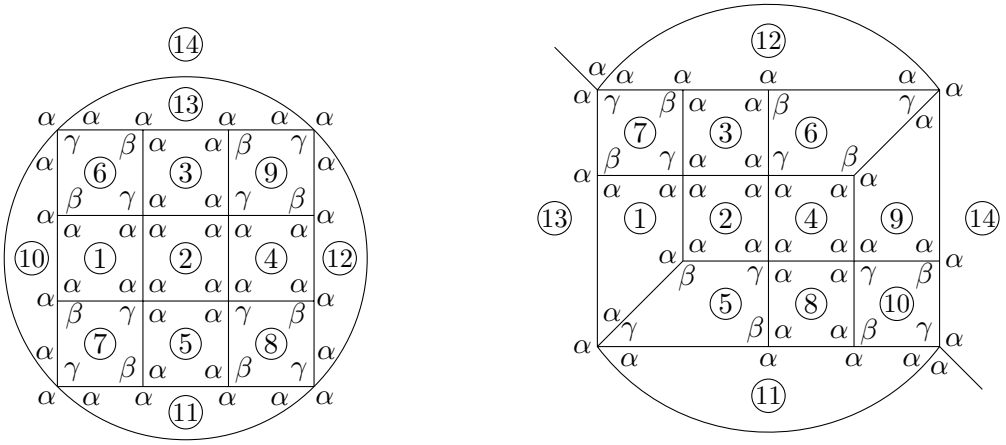

(a) (b)

Figure 4.10: The two tilings with AVC $\equiv \{\alpha^2\beta, \alpha^3\gamma\}$, 10 squares and 4 rhombi.

Proposition 4.6. *The edge-to-edge dihedral tilings of the sphere by the squares and the rhombi with a vertex $\beta^2\gamma$ are the infinite family of earth map type.*

Each member of the family has 2 squares and $4(2c-1)$ rhombi, where $c \geqslant 2$ is the number of γ's in $\alpha\beta\gamma^c$ (see Figures 2.3, 4.13).

Proof. Proposition 4.5 rules out $\alpha^2\beta$. The vertex angle sum of $\beta^2\gamma$ and $\beta > \alpha > \gamma$ imply $\beta^2\cdots = \beta^2\gamma$ and $\beta > \frac{2}{3}\pi$. Recall $\alpha > \frac{1}{2}\pi$. These facts imply that the possible vertex types are

$$\beta^2\gamma, \gamma^c, \alpha^{a\leqslant 3}\gamma^c, \beta\gamma^{c\geqslant 3}, \alpha\beta\gamma^{c\geqslant 2}.$$

Lemma 3.1 asserts that $\alpha\beta\cdots$ is a vertex and the above further implies $\alpha\beta\cdots = \alpha\beta\gamma^{c\geqslant 2}$. Hence $\alpha\beta\gamma^{c\geqslant 2}$ is a vertex.

We first rule out $\gamma^c, \alpha^a\gamma^c$ for our dihedral tilings.

The angle arrangement $\alpha|\gamma$ determines tiles T_1, T_2 in Figure 4.11. Then $\alpha_1\beta_2\cdots = \alpha\beta\gamma^{c\geqslant 2}$ determines T_3. The same argument also determines T_4, T_5. As we start with $\alpha|\gamma = \alpha_1|\gamma_2$, this implies $\alpha|\gamma\cdots = \beta|\alpha|\gamma\cdots = \alpha\beta\gamma^{c\geqslant 2}$, which rules out $\alpha^a\gamma^c$.

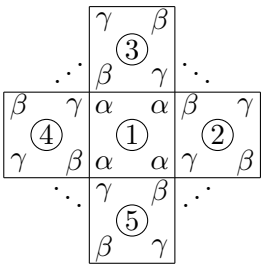

Figure 4.11: The deduction from $\alpha|\gamma$.

If γ^c is a vertex, then $\gamma|\gamma$ determines T_1, T_2 in Figure 4.12. Next, $\beta_1\beta_2\cdots = \beta^2\gamma$ determines T_3. The process continues at γ^c and eventually determines a monohedral earth map tiling $E^R_\square 1$ for each fixed $c \geqslant 3$ (see Figure 2.2 for $c = 3$). Hence γ^c is not a vertex in our dihedral tilings.

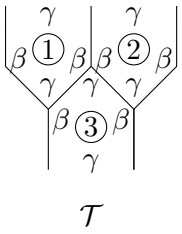

Figure 4.12: A time zone given by T_1, T_3 and $\mathcal{T} = c - \frac{1}{2}$ time zones for $c = 2$.

For $c \geqslant 2$, we use $\mathcal{T}$ to denote a block of $c - \frac{1}{2}$ time zones, equivalently $c - 1$ time zones plus one extra tile. Examples with $c = 2, 3$ are illustrated in Figure 4.12 and Figure 2.3a respectively.

The absence of $\gamma^c, \alpha^a\gamma^c$ implies

$$\text{AVC} = \{\beta^2\gamma, \beta\gamma^{c\geqslant 3}, \alpha\beta\gamma^{c\geqslant 2}\}. \tag{4.8}$$

At an $\alpha\beta\gamma^{c\geqslant 2}$, the same deduction from $\alpha|\gamma$ in Figure 4.11 determines the central square and its four vertices in Figure 4.13. For any fixed $c \geqslant 2$, the γ^c-part of each $\alpha\beta\gamma^{c\geqslant 2}$ determines a $\mathcal{T}$ in Figure 4.13a. The tiling is then completed by another square in the exterior of the "circular boundary". As instructed, it is straightforward to construct the minimal member ($c = 2$, Figure 4.13b) of the family.

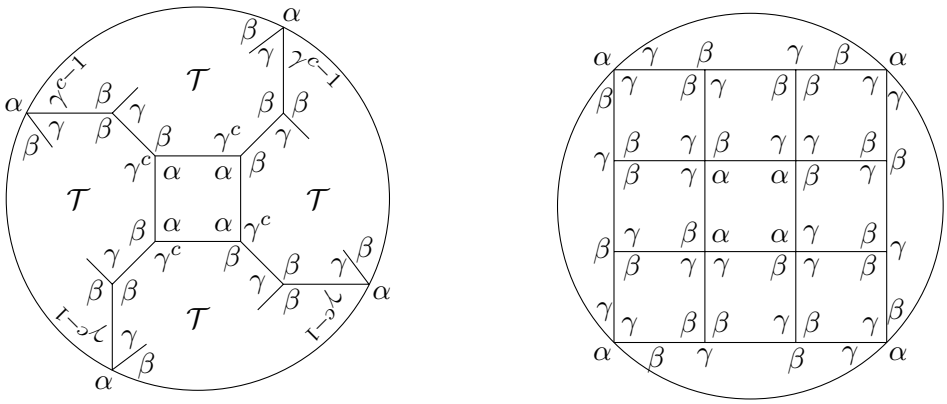

(a) $c \geqslant 2$ (b) $c = 2$

Figure 4.13: The tilings with $\beta^2\gamma, \alpha\beta\gamma^{c\geqslant 2}$ and 2 squares and $4(2c-1)$ rhombi.

The infinite family have the vertex types below

$$\text{AVC} \equiv \{\beta^2\gamma, \alpha\beta\gamma^{c\geqslant 2}\}, \tag{4.9}$$

meaning that $\beta\gamma^c$ does not appear as a vertex in the dihedral tilings. Note that, the monohedral tilings with AVC $\equiv \{\beta^2\gamma, \beta\gamma^c\}$ are the flip modification $FE^R_\square 1$ of $E^R_\square 1$ given by γ^c [CLY22, Proposition 23].

Lastly, we verify the geometric existence of the infinite family. The vertex angle sums of $\beta^2\gamma, \alpha\beta\gamma^c$ imply

$$\alpha = \pi - (c - \tfrac{1}{2})\gamma, \quad \beta = \pi - \tfrac{1}{2}\gamma. \tag{4.10}$$

The geometric existence of the tilings is equivalent to the existence of values for $\alpha, \beta, \gamma, x \in \mathbb{R}^+$ such that the constraints, (4.10), $0 < \cos x < 1$, (3.8), and $\pi > \beta > \alpha > \frac{1}{2}\pi > \gamma > 0$, are satisfied. As α, β are parametrised by γ in (4.10) and together with (3.8) the edge length x is also parametrised by γ, we will show that for every integer $c \geqslant 2$ that there exists a corresponding value $\gamma_c \in (0, \frac{1}{2}\pi)$ such that the above constraints are satisfied.

For $\gamma > 0$ and $c \geqslant 2$, the equations in (4.10) imply $\pi > \beta > \alpha$.

For $\gamma \in (0, \frac{1}{2}\pi)$, substituting the second equation of (4.10) into (3.8) gives

$$0 < \cos x = \tfrac{1}{2}(1 - \tan^2 \tfrac{1}{4}\gamma) < 1.$$

By (4.10) (the first equality), $\alpha > \frac{1}{2}\pi$ is equivalent to

$$(c - \tfrac{1}{2})\gamma < \tfrac{1}{2}\pi. \tag{4.11}$$

Meanwhile, substituting both equations in (4.10) into (3.6) gives

$$2\tan^2(2c-1)\tfrac{1}{4}\gamma + \tan^2 \tfrac{1}{4}\gamma - 1 = 0. \tag{4.12}$$

Now the geometric existence is equivalent to the following: for each integer $c \geqslant 2$ there exists a value for $\gamma_c \in (0, \frac{1}{2}\pi)$ such that (4.11), (4.12) hold for γ_c.

The general solution to (4.12) is

$$c_\pm = \pm\tfrac{2}{\gamma}(t(\gamma) + k\pi) + \tfrac{1}{2}, \qquad \text{where } t(\gamma) = \tan^{-1}\sqrt{\tfrac{\tan\frac{1}{4}\gamma}{\tan\frac{1}{2}\gamma}},\ k \in \mathbb{Z}.$$

For $\gamma \in (0, \frac{1}{2}\pi)$, we have $0 < t(\gamma) < \frac{1}{2}\pi$. This implies

$$c_+ \in (\tfrac{1}{2}, \tfrac{1}{2} + \tfrac{\pi}{\gamma}) + \tfrac{2k\pi}{\gamma},$$
$$c_- \in (\tfrac{1}{2} - \tfrac{\pi}{\gamma}, \tfrac{1}{2}) - \tfrac{2k\pi}{\gamma}.$$

For c to satisfy (4.11), it remains to consider $c(\gamma) = c_+$ with $k = 0$, i.e.,

$$c(\gamma) = \tfrac{2}{\gamma}t(\gamma) + \tfrac{1}{2}. \tag{4.13}$$

A plot of $c(\gamma)$ against $\frac{\gamma}{\pi}$ is given in Figure 4.14.

Now (4.13) implies that (4.11) is equivalent to $t(\gamma) < \frac{1}{4}\pi$. Since $\tan\theta$ is strictly increasing on $(0, \frac{1}{2}\pi)$, for $\gamma \in (0, \frac{1}{2}\pi)$ we have $\tan\frac{1}{4}\gamma < \tan\frac{1}{2}\gamma$ and hence $t(\gamma) < \frac{1}{4}\pi$ holds. Therefore (4.11) holds for $\gamma \in (0, \frac{1}{2}\pi)$.

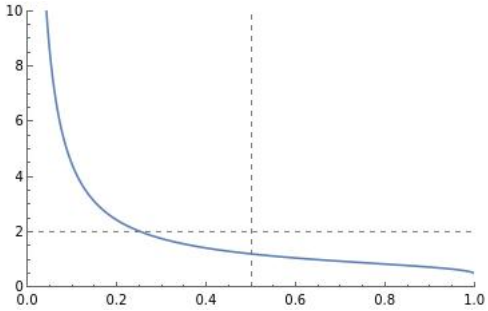

Figure 4.14: Graph of $c(\gamma)$ against $\frac{\gamma}{\pi}$.

Finally, it remains to show that, for any integer $c \geqslant 2$, there is a value $\gamma_c \in (0, \frac{1}{2}\pi)$ satisfying $c(\gamma_c) = c$. One can show that $c(\gamma)$ in (4.13) is continuous and decreasing on $(0, \frac{1}{2}\pi)$ and

$$\lim_{\gamma \to 0^+} c(\gamma) = +\infty.$$

On the other hand, we have

$$c(\tfrac{1}{2}\pi) = \tfrac{4}{\pi} t(\tfrac{1}{2}\pi) + \tfrac{1}{2} = \tfrac{4}{\pi} \tan^{-1}(\sqrt{\sqrt{2}-1}) + \tfrac{1}{2} < \tfrac{4}{\pi} \tan^{-1}(1) + \tfrac{1}{2} = \tfrac{3}{2}.$$

Here we get $c(\frac{1}{2}\pi) < 2$. The Intermediate Value Theorem guarantees that for any integer $c \geqslant 2$, there exists a γ_c as desired, which is also unique.

Therefore the infinite family of tilings in Figure 4.13 exist. By (4.10) and (4.12), we conclude with the numerical values of α, β, γ, x for $c = 2, 3$ below,

$$c = 2: \tag{4.14}$$
$$\alpha = (0.61456\ldots)\pi, \quad \beta = (0.87152\ldots)\pi, \quad \gamma = (0.25695\ldots)\pi, \quad x = (0.34097\ldots)\pi.$$
$$c = 3: \tag{4.15}$$
$$\alpha = (0.61045\ldots)\pi, \quad \beta = (0.92209\ldots)\pi, \quad \gamma = (0.15581\ldots)\pi, \quad x = (0.33610\ldots)\pi.$$

□

5. Conclusion and discussion

Strategy

Our strategy is to determine all the admissible vertex types in terms of incident angle combinations. To achieve this goal, the tools are built on local properties (e.g., vertex types of degree 3 (3.2), the trigonometric identity of the prototiles (3.6), etc.) and a global property (i.e., Counting Lemma). Based on the admissible vertex types, tilings are then constructed. What we demonstrate in this paper is a first extension of the machinery from [CLY22].

The studies of tilings with other prototile combinations may follow a similar path. For example, the strategy applies to a prototile combination consisting of a regular n-gon with $n \geqslant 5$ and a rhombus [CL24]. On the other hand, the prototile combination consisting of a regular triangle and a rhombus may also be studied analogously, possibly aided by computer.

Comparison

An interesting comparison is drawn by an anonymous reviewer between this classification and that of the monohedral tilings of the sphere by rhombi [CLY22, SA15]. Combinatorially, the 1-skeletons of the tilings from both sides are spherical maps with faces of size 4. Geometrically, there are isolated tilings and infinite families as realisations of these 1-skeletons. Differences are highlighted in terms of symmetry and modification.

The two isolated monohedral tilings by rhombi are given by the rhombic dodecahedron and rhombic triacontahedron. As shown in Figure 5.1, they can be deduced respectively from the octahedron (equivalently the cube) and the icosahedron (equivalently the dodecahedron) via the quadricentric subdivision [CLY22, the first main theorem]. From this viewpoint, their symmetries (octahedral and icosahedral) are obvious. Such symmetries are absent in our dihedral tilings as the squares and the rhombi fall in different orbits under an automorphism. Hence the dihedral tilings are not face-transitive. In addition, the octahedral symmetry of the truncated octahedron is "broken" by the quadrilateral subdivision on the hexagonal faces.

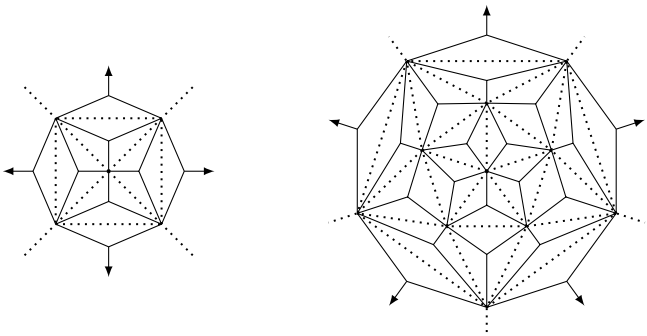

Figure 5.1: The rhombic dodecahedron via quadricentric subdivision CP_8 of the octahedron P_8 (in dotted lines); rhombic triacontahedron via quadricentric subdivision CP_{20} of the icosahedron P_{20} (in dotted lines).

In contrast to the dihedral tilings of Archimedean and sporadic types, the two monohedral tilings do not admit any modification. Nevertheless, the infinite monohedral families, $E^R_\square 1$ and $FE^R_\square 1$ in Figure 5.2, are related via a flip modification F [CLY22]. The time zone of the $E^R_\square 1$ (Figure 5.2) effectively forms the building blocks for both $E^R_\square 1$ and the infinite family in the main theorem (Figure 2.3), Section 2. The dihedral family however do not admit any modification. In general, the conditions allowing a tiling to admit a modification remain unclear.

"Near Misses"

It may be possible to conduct the arguments without (3.6) until the geometric realisation stage. Doing so leads to some "near misses" in which α, β, γ fail to satisfy (3.6). For example, the AVC $\equiv \{\alpha\beta^2, \alpha^3\gamma, \alpha\beta\gamma^2\}$ gives rise to the "non-geometric" tiling in Figure 5.3, and likewise for AVC $\equiv \{\alpha^2\beta, \beta^2\gamma, \alpha\beta\gamma^c\}$ in Figure 5.4. They are studied as tilings by "angle-congruent" polygons. Two polygons are *congruent* if there is a one-to-one correspondence between the

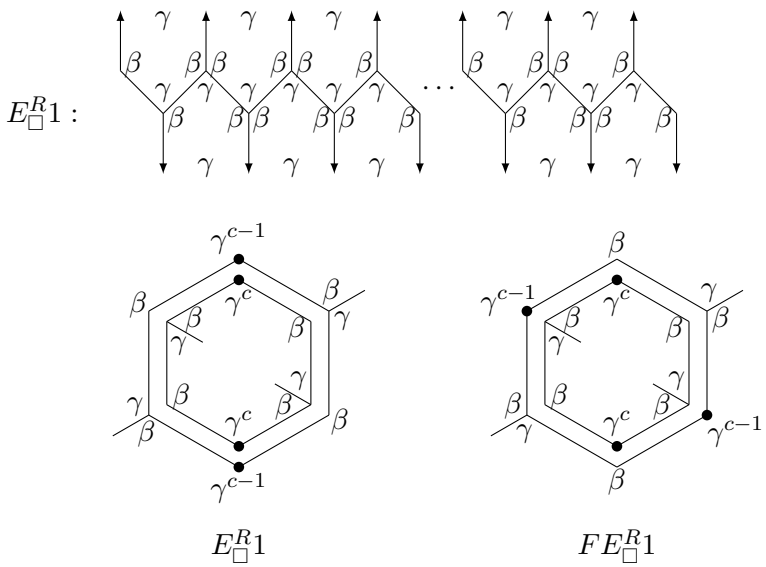

Figure 5.2: $E^R_\square 1$ with AVC $\equiv \{\beta^2\gamma, \gamma^{2c-1}\}$ and $FE^R_\square 1$ with AVC $\equiv \{\beta^2\gamma, \beta\gamma^c\}$.

angles and edges, such that the adjacencies of angles and edges are preserved and the corresponding angles and edges have equal values. If the polygons have the same correspondence except requiring corresponding edges to have equal values, they are called *angle-congruent*. In general, tilings by angle-congruent polygons do not necessarily have geodesic edges. The near misses are dihedral cases in point. Monohedral examples can be seen in [LY25].

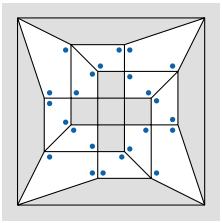

Figure 5.3: An angle-congruent tiling with $f = 22$, AVC $\equiv \{\alpha\beta^2, \alpha^3\gamma, \alpha\beta\gamma^2\}$, where $\bullet = \beta$.

We finish with an example of the infinite family in Figure 5.4. The two tilings in Figure 5.5 are the minimal member ($c = 2$ in $\alpha\beta\gamma^c$) and its flip modification. Both have two angle arrangements of $\alpha\beta\gamma^2$, $|\alpha|\beta|\gamma|\gamma|$ and $|\alpha|\gamma|\beta|\gamma|$. The latter appears in adjacent pairs in the second tiling and otherwise in the first.

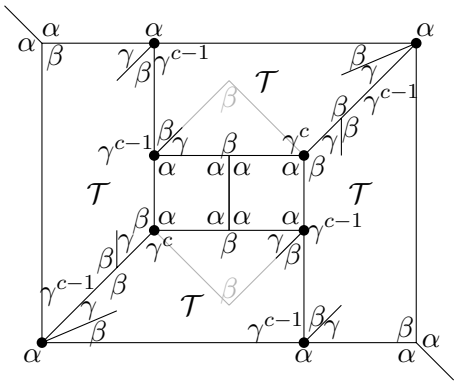

Figure 5.4: An infinite family of angle-congruent tilings with AVC $\equiv \{\alpha^2\beta, \beta^2\gamma, \alpha\beta\gamma^{c\geqslant 2}\}$, where $\mathcal{T}$ denotes the $c - \frac{1}{2}$ time zones in Figure 4.12.

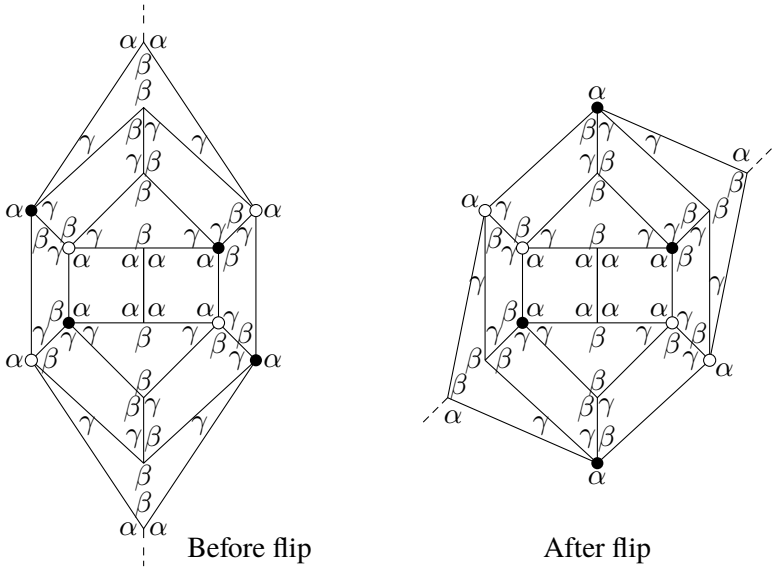

Figure 5.5: A flip modification relating angle-congruent tilings with AVC $\equiv \{\alpha^2\beta, \beta^2\gamma, \alpha\beta\gamma^2\}$, vertices $|\alpha|\beta|\gamma|\gamma|$ highlighted by $\bullet$ and $|\alpha|\gamma|\beta|\gamma|$ by $\circ$, the dashed lines in each picture connect to form one edge.

Acknowledgements

The author thanks the anonymous reviewers for their very helpful comments and suggestions. The author also extends his gratitude towards Min Yan, Roman Nedela, Ho Man Cheung, Chun Kit Kum and Christopher Purcell for the fruitful discussions. The author pays tribute to the late Jonas Evan Neubauer, the seven-time world champion and a wonderful human being: the T-piece argument was inspired by the game he loved and popularised.

The research was supported in part by the funding of Academic Career in Pilsen 2024 under Plzeňský kraj a Západočeská univerzita v Plzni.

References

[AEHJ24] C. Adams, C. Edgar, P. Hollander, and L. Jacoby. The non-edge-to-edge tilings of the sphere by regular polygons. *Discrete & Computational Geometry*, 72:1029–1085, 2024. doi:10.1007/s00454-024-00689-z.

[AHS18] Y. Akama, B. Hua, and Y. Su. Areas of spherical polyhedral surfaces with regular faces. 2018. arXiv:1804.11033.

[AS09] C. P. Avelino and A. F. Santos. Spherical f-tilings by scalene triangles and isosceles trapezoids, I. *European Journal of Combinatorics*, 30(5):1221–1244, 2009. doi:10.1016/j.ejc.2008.12.021.

[AWY22] Y. Akama, E. X. Wang, and M. Yan. Tilings of the sphere by congruent pentagons III: edge combination a^5. *Advances in Mathematics*, 394:107881, 2022. doi:10.1016/j.aim.2021.107881.

[AY23] Y. Akama and M. Yan. On deformed dodecahedron tiling. *Australasian Journal of Combinatorics*, 85(1):1–14, 2023.

[BR12] A. M. Breda and P. S. Ribeiro. Spherical f-tilings by two non congruent classes of isosceles triangles - I. *Mathematical Communications*, 17:127–149, 2012.

[BRS09] A. M. Breda, P. S. Ribeiro, and A. F. Santos. A class of spherical dihedral f-tilings. *European Journal of Combinatorics*, 30(1):119–132, 2009. doi:10.1016/j.ejc.2008.02.010.

[BS05] A. M. Breda and A. F. Santos. Dihedral f-tilings of the sphere by rhombi and triangles. *Discrete Mathematics and Theoretical Computer Science*, 7:123–142, 2005. doi:10.46298/dmtcs.348.

[CL21] H. M. Cheung and H. P. Luk. Tilings of the sphere by congruent quadrilaterals with exactly two equal edges. 2021. arXiv:2108.06574.

[CL24] H. M. Cheung and H. P. Luk. Dihedral tilings of the sphere by regular polygons and quadrilaterals II: regular polygons with high gonality and rhombi. 2024. arXiv:2403.07014.

[CLY22] H. M. Cheung, H. P. Luk, and M. Yan. Tilings of the sphere by congruent quadrilaterals or triangles. 2022. arXiv:2204.02736.

[CLY23] H. M. Cheung, H. P. Luk, and M. Yan. Tilings of the sphere by congruent pentagons IV: edge combination a^4b. 2023. arXiv:2307.11453.

[GSY13] H. H. Gao, N. Shi, and M. Yan. Spherical tiling by 12 congruent pentagons. *Journal of Combinatorial Theory, Series A*, 120(4):744–776, 2013. doi:10.1016/j.jcta.2012.12.006.

[Hig01] Y. Higuchi. Combinatorial curvature for planar graphs. *Journal of Graph Theory*, 38(4):220–229, 2001. doi:10.1002/jgt.10004.

[Joh66] N. Johnson. Convex solids with regular faces. *Canadian Journal of Mathematics*, 18:169–200, 1966.

[LC24] H. P. Luk and H. M. Cheung. Rational angles and tilings of the sphere by congruent quadrilaterals. *Annals of Combinatorics*, 28:485–527, 2024. doi:10.1007/s00026-023-00685-9.

[LCY24] H. P. Luk, H. M. Cheung, and M. Yan. Classification of edge-to-edge monohedral tilings of the sphere. In *Proceedings of Discrete Mathematics Days*, pages 89–94. Alcalá de Henares: Editorial Universidad de Alcalá, 2024. doi:10.37536/TYSP5643.

[Luk24] H. P. Luk. A parity phenomenon of spherical tilings. 2024.

[Luk25] H. P. Luk. Odd tilings of the sphere and graphs of Herschel type. 2025.

[LY25] H. P. Luk and M. Yan. Angle combinations in tilings of the sphere by angle congruent pentagons. *Graphs and Combinatorics*, 41:33, 2025. doi:10.1007/s00373-024-02879-1.

[Nv14] R. Nedela and M. Škoviera. *Maps*. Handbook of Graph Theory, Second Edition. Chapman and Hall/CRC, 2014.

[SA15] Y. Sakano and Y. Akama. Anisohedral spherical triangles and classification of spherical tilings by congruent kites, darts and rhombi. *Hiroshima Mathematical Journal*, 45(3):309–339, 2015. doi:10.32917/hmj/1448323768.

[SMKGS24] D. Smith, J. S. Myers, C. S. Kaplan, and C. Goodman-Strauss. An aperiodic monotile. *Combinatorial Theory*, 4(1):6, 2024. doi:10.5070/C64163843.

[Som24] D. M. Y. Sommerville. Division of space by congruent triangles and tetrahedra. *Proceedings of the Royal Society of Edinburgh*, 43:85–116, 1924. doi:10.1017/S0370164600022495.

[Tod86] I. Todhunter. *Spherical Trigonometry*. MacMillan, 1886.

[UA02] Y. Ueno and Y. Agaoka. Classification of tilings of the 2-dimensional sphere by congruent triangles. *Hiroshima Mathematical Journal*, 32(3):463–540, 2002. doi:10.32917/hmj/1151007492.

[WY22a] E. X. Wang and M. Yan. Tilings of sphere by congruent pentagons I: edge combinations a^2b^2c and a^3bc. *Advances in Mathematics*, 394:107866, 2022. doi:10.1016/j.aim.2021.107866.

[WY22b] E. X. Wang and M. Yan. Tilings of sphere by congruent pentagons II: edge combination a^3b^2. *Advances in Mathematics*, 394:107867, 2022. doi:10.1016/j.aim.2021.107867.

[Yoo12] K. Yoon. Analytical calculation of geodesic lengths and angle measures on sphere tiling of platonic and archimedean solids. In *Proceedings of Bridges Towson 2012: Mathematics, Music, Art, Architecture, Culture*, pages 509–512. MathArtFun, 2012.

[Zal67] V. Zalgaller. Convex polyhedra with regular faces. *Zap. Nauchn. Semin.Leningr. Otd. Mat. Inst. Steklova*, 2:1–221, 1967.